Article

Journal of
Biomedical Nanotechnology
Vol. 12, 1–12, 2016
www.aspbs.com/jbn

Mineralized Collagen Regulates Macrophage Polarization During Bone Regeneration

Yue Sun[1], Shuai Liu[1], Yu Fu[1], Xiao-Xing Kou[1], Dan-Qing He[1], Gao-Nan Wang[1], Cui-Cui Fu[2], Yan Liu[1,*], and Yan-Heng Zhou[1,*]

[1] *Center for Craniofacial Stem Cell Research and Regeneration, Department of Orthodontics, Peking University School and Hospital of Stomatology, Beijing 100081, P. R. China*
[2] *Department of Orthodontics, The Fourth Affiliated Hospital of Zhengzhou University, Henan 450000, P. R. China*

The host immune response to bone biomaterials is vital in determining the fate of scaffolds and also the outcomes of bone regeneration. Mineralized collagen is an ideal tissue-engineering scaffold for bone repair; however, little is known about its immunomodulatory properties after implantation. In this study, extrafibrillarly-mineralized collagen (EMC) and intrafibrillarly-mineralized collagen (IMC) scaffolds with different nanostructures were fabricated and their immunomodulatory properties via macrophage polarization during bone regeneration were investigated. Micro-CT findings showed that the IMC scaffold yielded more new bone formation than the EMC scaffold. In the defect area, more CD68+CD163+M2-like macrophages were observed in the IMC group, while M1-like macrophages positive for CD68 and inducible nitric oxide synthase (iNOS) increased dramatically in the EMC group. We further demonstrated, from the protein and RNA levels, that M2-associated anti-inflammatory cytokines interleukin (IL)-10 and arginase-1 were highly expressed in the macrophages seeded on the IMC scaffold, while those seeded on the EMC scaffold expressed more M1-related genes iNOS and IL-6. Moreover, the macrophage polarization in response to the nanostructure of mineralized collagen scaffolds influenced the osteogenesis of human bone marrow stromal cells. These findings suggest that the nanostructure of mineralized collagen scaffolds affects macrophage functional polarization during bone regeneration. The immunomodulatory properties of biomaterial scaffolds can be a dictator of bone regeneration outcomes.

KEYWORDS: *Macrophage Polarization, Nanostructure, Intrafibrillarly-Mineralized Collagen, Extrafibrillarly-Mineralized Collagen, Tissue Engineering.*

INTRODUCTION

Tissue engineering and regenerative medicine have created an increasing demand for bone substitute materials due to limitations of the availability and morbidity of autologous grafts.[1–3] Since the host immune reactions following biomaterial implantation regulate osteogenesis to affect the outcomes of new bone regeneration, the paradigm for the design of bone substitute materials has been shifted from being relatively inert (minimizing the host response) to having immunomodulatory properties.[4,5]

Macrophages, a major constituent part of the innate immune system, are responsible for recruiting other immune cells to the inflamed site and activating both the complement and adaptive immune system.[6] They are the first to respond to the implantation of biomaterials[7,8] and play a vital role in mediating tissue remodeling. The activated macrophages exhibit a spectrum of polarization states.[9,10] At one end of the spectrum, classically activated (M1) macrophages stimulated by interferon (IFN)-γ or lipopolysaccharide (LPS) promotes inflammation by producing high levels of inducible nitric oxide synthase (iNOS) and pro-inflammatory cytokines such as interleukin (IL)-6 and tumor necrosis factor (TNF)-α. The other end is alternatively activated (M2) macrophages activated by IL-4 or IL-13, can produce anti-inflammatory and pro-healing cytokines, such as IL-10 and arginase-1.[10–15] It has been established that the ratio of M1/M2 can affect the outcomes of tissue regeneration after scaffold implantation.[16–20] The prolonged presence of M1 macrophages will lead to the damage of the biomaterial and impair its capacity to promote tissue regeneration.

*Authors to whom correspondence should be addressed.
Emails: orthoyan@bjmu.edu.cn, yanhengzhou@gmail.com
Received: 11 December 2015
Accepted: 15 March 2016

Therefore, a subsequent transition to M2 phenotype, which promotes tissue remodeling, is believed to be a favorable adaptation.[18–20]

The host macrophage response is an essential element of the tissue remodeling process following the implantation of biomaterials, and macrophage polarization has been acknowledged to be a key modulator of the tissue remodeling process.[21–25] Physical properties of biomaterials, such as nanostructure, stiffness, and pore size can dictate the host response and macrophage polarization.[26–31] Moreover, the outcomes of bone regeneration could be improved by incorporating scaffolds with M1/M2-associated cytokines.[28, 32–35] Mineralized collagen, which composes the basic nanostructure of bone extracellular matrix (ECM),[29] is believed to be the ideal scaffold in bone tissue engineering. In our previous studies,[36–39] intrafibrillarly-mineralized collagen mimicking bone nanostructure was successfully fabricated[38] and the nanostructure of mineralized collagen influenced its cytocompatibility and osteogenic potential.[39] Since the immunomodulatory properties of biomaterials is a dictator of bone regeneration outcomes, in the present study, the rat mandibular critical-size defect (CSD) animal model was used to first investigate the effect of nanostructure of mineralized collagen on bone regeneration *in vivo*, and to further reveal host macrophage response to the nanostructure of mineralized collagen.

MATERIALS AND METHODS

Preparation and Characterization of Mineralized Collagen Scaffolds

Mineralized collagen scaffolds were prepared as previously reported.[39] Briefly, type I tropocollagen solution from rat tails (Corning®, 10 mg/ml) contained in a dialysis membrane (3500 Da) was immersed in a flask, which contained 1 g of set type I white Portland cement (Lehigh Cement Co., Allentown, PA, USA) as a calcium source, 15 ml of simulated body fluid (136.8 mM NaCl, 4.2 mM $NaHCO_3$, 3.0 mM KCl, 1.0 mM $K_2HPO_4 \cdot 3H_2O$, 1.5 mM $MgCl_2 \cdot 6H_2O$, 2.5 mM $CaCl_2$, 0.5 mM Na_2SO_4 and 3.08 mM Na_3N) as a phosphate source and 0.5 mg/ml of poly(acrylic acid) (PAA, Mw 2000, Sigma-Aldrich) as a stabilizer of amorphous calcium phosphate. The hydroxyapatite/collagen fibrils co-precipitations were carried out at 37 °C for 7 days and intrafibrillarly-mineralized collagen (IMC) was achieved. In the absence of PAA in the mineralization solution, extrafibrillarly-mineralized collagen (EMC) was obtained. To prepare 3-D scaffolds, the mineralized collagen deposition was collected by centrifugation and stirred until a just-castable suspension was formed. Then, the suspension was poured into the cavities of 48-well polystyrene culture plates, frozen at −30 °C for 24 h and lyophilized to form sponge-like porous collagen scaffolds for morphology test and animal experiment.

The micro- and nano-structure of the collagen scaffolds was observed by scanning electron microscopy (SEM) and transmission electron microscopy (TEM) respectively. For SEM examination, samples were dehydrated in graded series of ethanol (50, 70, 80, 85, 90, 95 and 100%), critical-point dried, and sputter-coated with gold for 2 min at 20 mA and observed by SEM at 15 kV (Hitachi S-4800, Japan). For TEM examination, samples were embedded in epoxy resin, sectioned with an ultramicrotome (Leica) and collected on copper grids.

Animal Models

A critical-sized defect[40, 41] (5 mm in diameter) was created in Sprague-Dawley (180–200 g, 6–7 weeks old) rat mandibles to evaluate the bone regeneration by mineralized collagen scaffolds. The experimental protocols were approved by the Animal Use and Care Committee of Peking University (LA2012-77). The EMC and IMC scaffolds were randomly placed into the defect area and the control group was with no scaffold ($N = 5$). After two, four and eight weeks of implantation, rats were sacrificed by over-anesthesia, and the mandibles were obtained and fixed in 4% paraformaldehyde.

Micro-Computed Tomography (CT) Analysis

The samples were scanned with a micro-CT system (Inveon MMCT, SIEMENS, USA) at 80 kV and 500 μA. Inveon Research Workplace (SIEMENS, USA) was used for 3D image reconstruction and the measurement of new bone formation can be done automatically by the system (gray value > 1000). The measurement was taken 3 times by a trained researcher blinded to the group design.

Histomorphologic Observation by Hematoxylin and Eosin (H&E) Staining

The samples were demineralized in 15% ethylenediaminetetraacetic acid, and then embedded by paraffin. Consecutive horizontal sections (5 μm in thickness) were obtained from the middle sagittal plane of the defect area. The sections were deparaffinized with xylene followed by exposure to a graded series of ethanol solutions (70%–100%) and then stained with hematoxylin and eosin (HE) and dehydrated using the reverse of the deparaffinization treatment prior to coverslip.

Immunofluorescence Staining

Sections were incubated overnight at 4 °C with antibodies of anti-CD68 (1:600; MCA341GA, AbD Serotec, UK) for pan-macrophage marker, and anti-iNOS (1:100; ab-15323, Abcam) or anti-CD68 and anti-CD163 (1:100; sc-33560, Santa Cruz) to detect M1- or M2-like macrophages, respectively. After extensive washing with phosphate buffer saline (PBS, 0.1 M), the sections were incubated for 30 min at room temperature with the respective fluorescein isothiocyanate-conjugated or tetramethylrhodamine

isothiocyanate-conjugated secondary antibody (1:200, Zhongshan Golden Bridge Biotechnology, Beijing, China). Nuclei were counterstained with 4′,6-diamidino-2-phenylindole (DAPI). Confocal microscopic images were acquired using a Zeiss laser-scanning microscope (LSM 510), and the images were processed with the Zen software. For semiquantification, the ratios of double-labeled positive cells and M1/M2 were calculated ($N = 5$) 3 times by a trained researcher who was blinded to the group design.

Immunohistochemistry

Immunohistochemistry was performed with a 2-step detection kit (Zhongshan Golden Bridge Biotechnology, Beijing, China). Briefly, sections were subjected to antigen retrieval with 0.125% trypsin and 20 μg/ml proteinase K solution at room temperature for 20 min. The sections were then blocked with 5% BSA for 30 min at room temperature and incubated overnight at 4 °C with antibodies against rat IFN-γ (1:50; sc-1377, Santa Cruz) for a M1 marker, and IL-4 (1:100; sc-53084, Santa Cruz) for a M2 marker. After extensive washing with PBS, the sections were incubated with Horseradish Peroxidase-conjugated secondary antibodies and visualized using diaminobenzidine (Zhongshan Golden Bridge Biotechnology, Beijing, China). Each group is composed of more than 3 slides and each slide was observed at the defect area including the scaffolds ($N > 3$).

In Vitro Human Macrophage Response to Different Mineralized Collagen Scaffolds

Cell Culture

THP-1 human monocytic cells were used to differentiate into macrophages on the coated slips or 6-well plates with RPMI 1640 medium (Gibco, USA) containing 10% fetal bovine serum (Equitech Bio Inc., USA), 1% penicillin/streptomycin and 50 ng/ml phorbol myristate acetate (PMA; P1585, Sigma, USA) for 24 h at 37 °C, 5% CO_2. The mineralized collagen precipitations (2 mg/ml) were collected on the cover slips (15 mm in diameter) pretreated with polylysine or 6-well plates and cross-linked with 0.3 M 1-ethyl-3(3-dimethylaminopropyl)-carbodiimide and 0.06 M N-hydroxysuccinimide to stabilize the scaffolds. The coated slips or 6-well plates were sterilized by soaking in the 75% ethanol for 2 hours and then under ultraviolet light for 2 hours before use. After we have generated adherent THP-1 derived macrophage, cells were cultured for 1, 3, and 7 days for time-course detection of macrophage polarization.

Macrophage Morphology Analysis

THP-1 cells were seeded on the EMC and IMC coated cover slips put in 24-well plates (2×10^4 cells per well) while the polylysine-treated coverslip was used as control. Add 50 ng/ml PMA for 24 h in the culture medium to create adherent cells, and then cells were kept culturing for 1 day to fully interact with the scaffolds. For SEM observation, samples were fixed in 3.7% glutaraldehyde and dehydrated in a graded ethanol series (30%, 50%, 70%, 80%, 85%, 90%, and 100%) and observed under SEM at 15 kV (Hitachi S-4800, Japan). For laser scanning confocal microscopy (LSM510, Zeiss, Jena, Germany), samples were fixed in 4% paraformaldehyde and then stained with Alexa Fluor 488 Phalloidin (F-actin, green). After washing twice, the cells were mounted with mounting media containing DAPI (blue) for nuclei staining and viewed by LSM.

Cytokine Measurements by Enzyme-Linked Immunosorbent Assay (ELISA)

The supernatants of cultured THP-1 derived macrophages on different mineralized collagen scaffolds were collected at 1, 3, and 7 days and stored at −80 °C before use. We detected the secretion of M1-associated cytokine, iNOS and IL-6, and the M2-assocatiated cytokine, IL-10 and arginase-1, by using ELISA kits (R&D systems, Minneapolis, USA) according to the manufacturer's instructions.

Quantitative Real-Time Polymerase Chain Reaction (PCR)

Total RNA was isolated from cell lysate with Trizol reagent (Invitrogen, Carlsbad, CA) and the synthesis of cDNA was performed using SuperScript® III One-Step RT-PCR System with Platinum® Taq High Fidelity (Invitrogen). The synthesized cDNA was stored at −20 °C until use.

Real-time PCR was performed on a 7900HT Fast Real Time PCR machine (Applied Biosystems) using SYBR Green (Invitrogen Life Technologies). The primers designed by primer premier 5.0 software and commercially synthesized were as follows:

Human-GAPDH	ATGGGGAAGGTGAAGGTCG GGGGTCAT TGATGGCAACAATA
Human-IL-6	GACCCAACCACAAATGCCA GTCATGTCCTGCAGCCACTG
Human-iNOS	ATTCACTCAGCTGTGCATCG TCAGGTGGGATTTCGAAGAG
Human-IL-10	TCAAGGCGCATGTGAACTCC GATGTCAAACTCACTCATGGCT
Human-arginase-1	CTTGGCAAAAGACTTATCCTTAG ATGACATGGACACATAGTA CCTTTC

The efficiency of the newly designed primers was confirmed by sequencing the conventional real-time PCR products.

Human Bone Marrow Stromal Cells (hBMSCs) Cultured with THP-1 Supernatants

To detect the correlation between macrophage polarization and the osteogenesis of hBMSCs, we cultured the hBMSCs with the supernatant of THP-1 derived macrophages seeded on different scaffolds. HBMSCs were isolated using a previously described method[42] and the protocol was approved by the Ethical Guidelines of Peking University (PKUSSIRB-201311103). Briefly, the marrow cells from mandible trabecular bone were released into culture dishes, processed by repeated pipetting and passaged through needles to disperse the cells followed by subsequent filtration through a 70 μm nylon cell strainer (BD Bioscience, USA). The hBMSCs were cultured in α-MEM supplemented with 20% fetal bovine serum (Equitech Bio Inc., USA), 1% penicillin/streptomycin and 2 mM glutamine (Gibco, USA).

THP-1 human monocytic cells (1×10^6) were used to differentiate into macrophages by PMA in coated 6-well plates (as former mentioned Cell Culture) and the supernatants of different groups were collected at 7 days. Then the hBMSCs were cultured with the supernatant for 7 days. Alkaline phosphatase (ALP), osteocalcin (OCN) and Runt-related transcription factor 2 (RUNX2), the osteogenic genes were evaluated by real-time PCR as stated before (Quantitative Real-Time Polymerase Chain Reaction). The primers designed by primer premier 5.0 software and commercially synthesized were as follows:

Human-OCN	CCCAGGCGCTACCTGTATCAA
	GGTCAGCCAACTCGTCACAGTC
Human-ALP	CCTTGTAGCCAGGCCCATTG
	GGACCATTCCCACGTCTTCAC
Human-Runx2	CACTGGCGCTGCAACAAGA
	CATTCCGGAGCTCAGCAGAATAA

Statistical Analysis

Statistical analysis was performed with SPSS 13.0. All data were presented as mean $\pm$ standard deviation and assessed by one-way ANOVA. Statistical significance was considered at $P < 0.05$.

RESULTS

Characterization of Mineralized Collagen

3-D porous collagen scaffolds with interconnected pores of 107.45 ± 8.67 μm were fabricated using a homogeneous freeze-drying process (Figs. 1(A, D)). In the EMC scaffold (Figs. 1(A–C)), apatite clusters randomly deposited around the surface of collagen fibrils (93.9 ± 13.7 nm). Typical cross-banding patterns (67 nm) could be observed in the fibrils (213.2 ± 12.1 nm) in the IMC scaffold indicated by SEM (Figs. 1(D, E)) and TEM (Fig. 1(F)). The increased diameter of the IMC fibril might be attributed to the substitution of the free water inside the collagen fibril by intrafibrillar apatites.

Bone Volume and Histomorphologic Observations

A CSD with 5 mm diameter mandible defect was created and micro-CT was applied to evaluate the new bone formation after implantation of different scaffolds. Fibrous bone structures could be seen in the center of the defect area by 8 week of implantation of the IMC scaffold, while only limited bone formation was seen along the defect margin in the EMC group (Fig. 2). The HE staining showed that new bone formed both at the defect margin and in the middle of the defect area in the IMC group while the EMC group showed more fibrous tissue surrounding the scaffolds and limited newly-formed bone at the margin. The defect area of the control group hardly changed through all time points indicating a reliable animal model (Fig. 3(A)). The quantitative data (Fig. 3(B)) showed bone volume of the defect area was significantly higher for the IMC group when compared to the EMC group at all time points.

M1/M2 Macrophage Ratio

M1-/M2-like macrophage infiltration was detected by immunofluorescence staining at each time point of both groups (Figs. 4(A, B)). In the IMC group, CD68 + CD163 + M2-like macrophages were remarkably dominant in the defect area. The numbers of M2 macrophages increased dramatically in the IMC group and arrived a peak at 8 weeks while CD68 + iNOS + M1-like macrophages remains a significantly low level during the whole time course. On the contrary, the EMC group showed an opposite situation that much more M1-like macrophages infiltrated in the defect area at all time points. The M1/M2 macrophage ratio (Fig. 4(C)) indicated predominance of M1 macrophages in the EMC group (ratio > 1) whereas the IMC scaffold induced predominant M2 macrophages (ratio < 1). These data indicated that EMC scaffold could provoke more M1 macrophage polarization while IMC scaffold showed more M2 macrophage polarization.

To further investigate the different macrophage polarization, the M1 (IFN-γ) and M2 (IL-4) inducer were detected respectively in the defect area among all time points (Fig. 4(D)). The EMC group exhibited high expression level of IFN-γ and low expression level of IL-4. By contrast, IL-4 was detected with higher expression level at all time points while only a few IFN-γ positive cells infiltrated in the IMC group at 2 and 4 weeks.

Macrophage Morphology

SEM and LSM were combined to observe the morphology of macrophages seeded on the mineralized collagen scaffold. The macrophages seeded on the glass slide (Figs. 5(A, D)), showed a sphere-like appearance, indicating a non-activated state. The SEM images (Figs. 5(B, C)) showed the macrophages adhered to the surface of the mineralized collagen well. However, the apatite clusters in the EMC scaffold seemed to impair

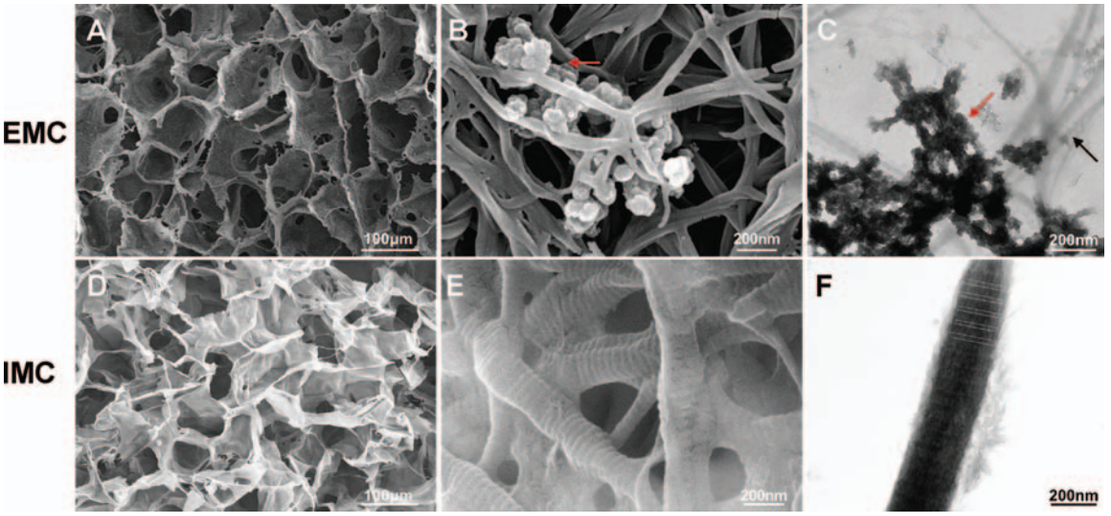

Figure 1. **The micro- and nano-structure of mineralized collagen scaffolds characterized by SEM and TEM (A, D). The EMC and IMC porous scaffolds showed similar interconnected pores of 107.45 ± 8.67μm (B, C). In the EMC scaffold, apatite clusters (red arrow) randomly deposited around the surface of unmineralized collagen fibrils (93.9 ± 13.7 nm, black arrow), which showed low electron density. In the IMC scaffold (E, F), a typical cross-banding pattern with 67 nm was identified and the collagen fibrils (213.2 ± 12.1 nm) showed high electron density.**

the macrophage elongation and migration while in the IMC group macrophages extended more freely and tended to have a polarized morphology. The representative images of actin immunofluorescence staining (Figs. 5(E, F)), consistent with the SEM, showed that macrophages on the EMC scaffold remained a round, oval shape whereas on the IMC scaffold appeared spindle-like polarized shape.

Inflammatory Gene Expression and Cytokine Secretion

THP-1 derived macrophages seeded on the EMC scaffold showed a M1 macrophage polarization with high expression of the M1-related gene, iNOS (Fig. 6(A)) and IL-6 (Fig. 6(B)). By contrast, macrophages seeded on the IMC scaffold emerged a significant shift toward high expression of IL-10 and arginase-1, indicating an M2 macrophage polarization.

Furthermore, the concentrations of the M1/M2-associated cytokines were detected with ELISA. The EMC group, with remarkably elevated levels in iNOS (Fig. 7(A)) and IL-6 (Fig. 7(B)), presented an M1 macrophage profile. Nevertheless, the IMC group showed significantly increased secretion of IL-10 (Fig. 7(C)) and arginase-1 (Fig. 7(D)), indicating an M2 macrophage polarization. These findings correspond with the immunofluorescence staining results *in vivo*, where the EMC scaffold showed more M1-like macrophage as the IMC scaffold showed more M2-like macrophage infiltration.

Osteogenic Potential of hBMSCs

THP-1 derived macrophages were seeded on the EMC and IMC scaffolds and the supernatant was added to the hBMSCs to further evaluate their osteogenic potential by measuring mRNA expression levels of bone-related markers including ALP, OCN and RUNX2 (Fig. 8). In the absence of any osteogenic induction, the expression levels of those genes were upregulated in the IMC group profoundly compared to the control group and the EMC group. The mRNA level of ALP (an early osteogenic marker) was remarkably upregulated by nearly four-fold. However, the EMC group with respect to the control group did not significantly affect the mRNA levels of those genes. These data indicated that macrophages in response to the IMC scaffold could promote osteogenic potential of hBMSCs remarkably.

DISCUSSIONS

The host immune response after the biomaterials implantation arise a profound impact on the host immune response;[43,44] meanwhile, the immune response is of primary importance in determining the quality of the bone regeneration. In this study, two mineralized collagen scaffolds with different nanostructure were fabricated to examine the bone regeneration outcomes and their immunomodulatory properties were evaluated by detecting macrophage response *in vivo* and *in vitro*. Owing to the nanostructure of the mineralized collagen scaffolds, the macrophages polarized differently, which might render them perform distinctly in bone regeneration.

Macrophages can switch polarization states in response to their local environment[24,45,46] such as surrounding cells or ECM. The properties of biomaterial scaffold can modulate the macrophage microenvironment and eventually affect macrophage polarization.[45,46] Many *in vitro* studies

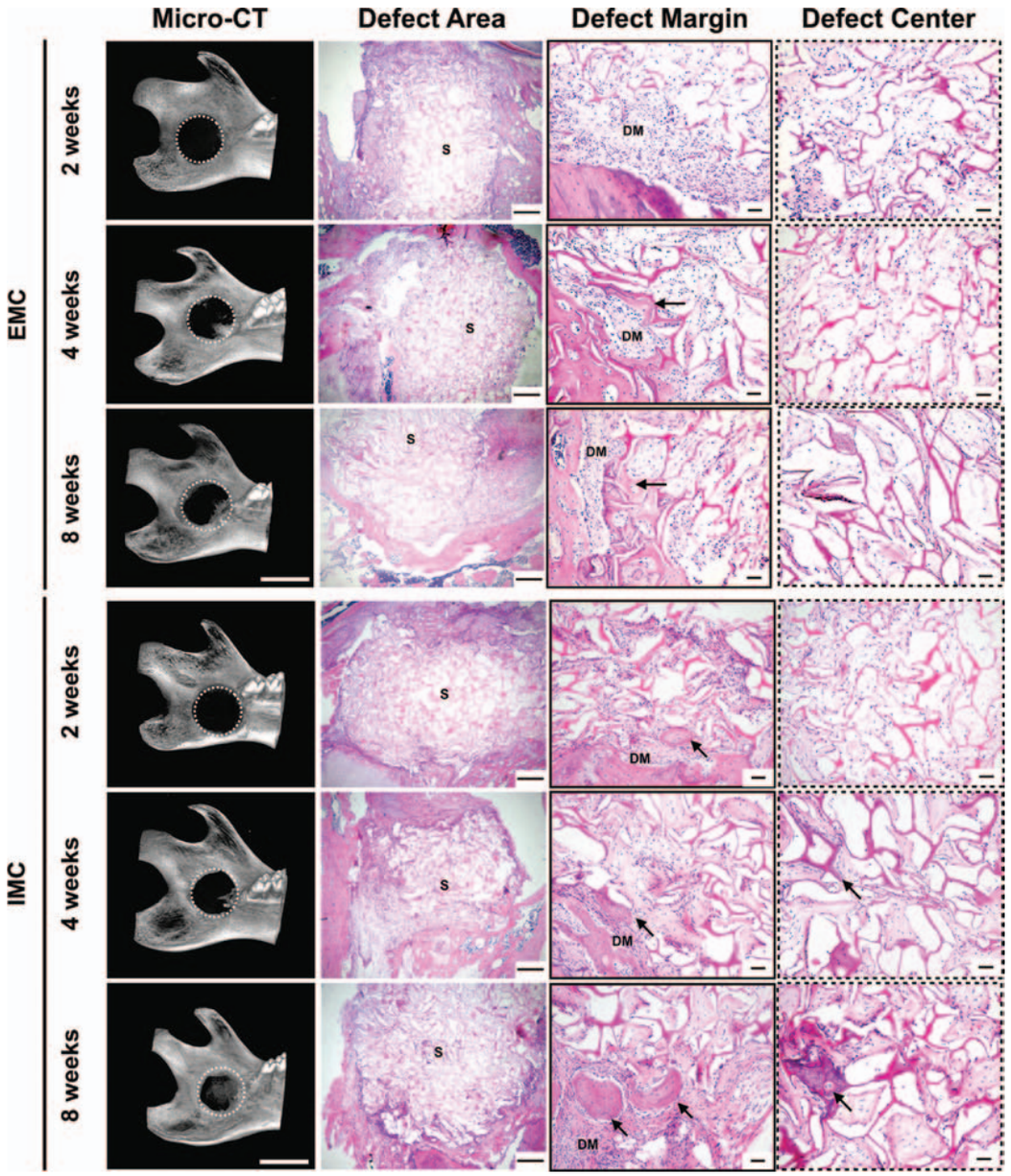

Figure 2. **Bone regeneration by the EMC and IMC scaffolds at different time points. The representative micro-CT images showed the IMC scaffolds yielded more new bone than the EMC scaffolds at each time point (Scale bar = 5 mm). Histomorphology of the defect area showed new bone (black arrow) formed both at the margin (DM) and in the middle of the defect area in the IMC group while the EMC group showed more soft fibrous tissue around the scaffolds (Scale bar = 1 mm for the defect area, Scale bar = 100 μm for the defect margin and defect center).**

have illustrated that the nanostructure of scaffold surface and mechanical stiffness can mediate changes in cytoskeleton reorganization[47] and regulate the transition between different macrophage phenotypes.[48–51] In our *in vivo* study, we found that the nanostructure of mineralized collagen scaffolds affected bone regeneration, accompanied with different macrophage polarization. The IMC scaffold, mimicking the nanostructure of natural bone, improved new bone formation and favored the M2 macrophage polarization.[21,22,52] It has been shown that the M1 to M2 transition contributes to stabilize growing blood vessels and promote tissue remodeling[53,54] and more downstream effects. Therefore, the modulation of macrophage polarization can be a predictor for constructive remodeling following the scaffold implantation.[17–19]

Macrophage morphology could reflect their functional status: polarized or stretched cells are considered activated, whereas static oval-like macrophages are considered inactivated.[55] Furthermore, macrophages polarized toward different phenotypes exhibit dramatic changes in

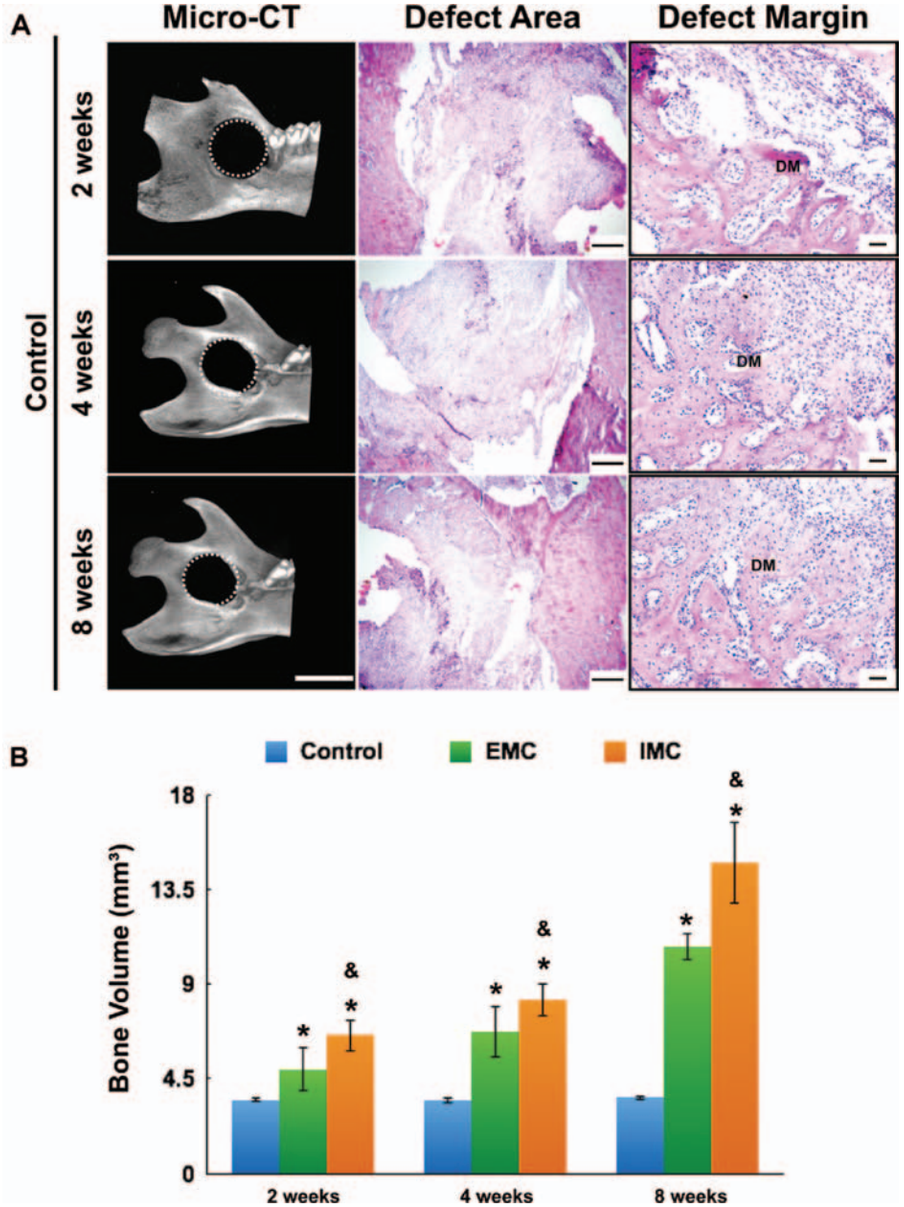

Figure 3. **(A) The representative micro-CT and H&E staining images showed the defect area in the control group was occupied with soft fibrous tissue and little new bone formation was observed. (B) Bone volume of the mandible defect area in different groups. Bone volume in the IMC group significantly increased at 2, 4, 8 weeks compared to that in the control and the EMC group. $N = 5$; $^{*}P < 0.05$ versus control, $^{\&}P < 0.05$ versus EMC.**

cell shape: M1 macrophages assume a round shape while M2 cells exhibit an elongated shape.[56] In the present study, macrophages adhered to the EMC and IMC scaffolds, but exhibited different morphology. The cells seeded on the IMC scaffold spread more freely and presented more spindle-like pseudopodia compared to those seeded on the EMC scaffold. This might be attributed to the distinguished nanotopography of the mineralized collagen scaffold, which is similar to previous studies.[33–35, 44, 49] The macrophage morphology has been proven highly relevant to its functional phenotype.[55, 56] This is evidenced by our real time-PCR and ELISA results, which suggested that macrophages seeded on the IMC scaffold, presented an M2-like macrophage profile while those seeded on the EMC scaffold, showed an M1-like macrophage profile. The "topography-induced polarization" seemed to provide us a new way to unravel the underlie mechanisms of how the IMC or EMC scaffold provoke different macrophage polarization *in vivo*.

Although macrophages have been shown to be involved in osteogenesis, and the M2 phenotype seemed to lead to better outcomes of bone regeneration, no consensus

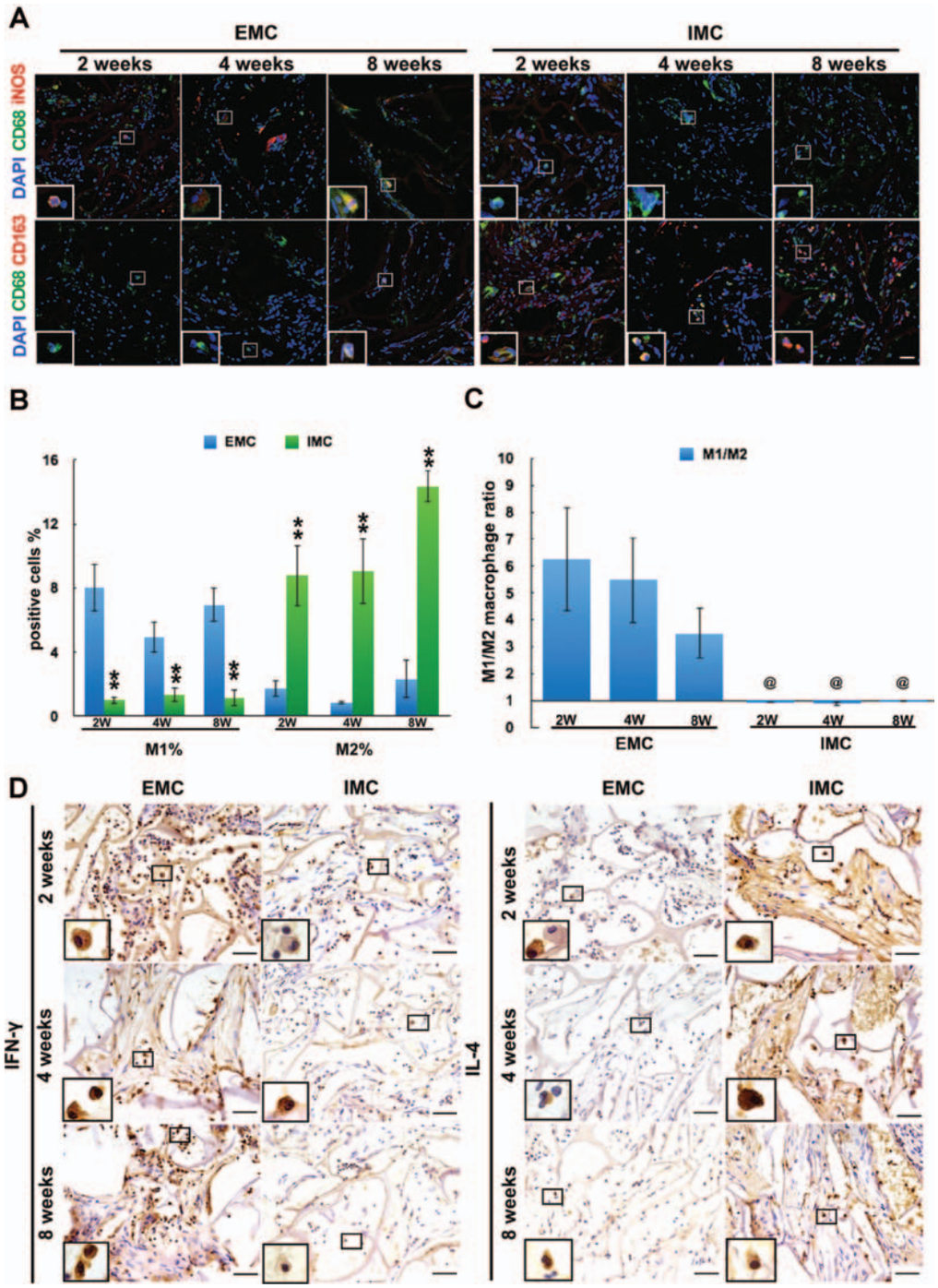

Figure 4. Macrophage polarization regulated by mineralized collagen in the defect area. (A) Representative immunofluorescence images of defect area. The EMC group showed more CD68 + (green) and iNOS + (red) M1-like macrophages (merge as yellow) infiltrated whereas the IMC group presented a significantly dominance of CD68 + (green) and CD163 + (red) M2-like macrophages (merged as yellow). Large boxed area showed the high-magnification views of the small-boxed area. Scale bar = 100 μm. (B, C) Semiquantification of the double-stained positive cells. M1 macrophages dominated in the EMC group while M2 macrophages contributed the major proportion in the IMC group. $N = 6$, positive cells %: $^{**}P < 0.01$ versus EMC at the same time point; M1/M2 ratio: $^{@}P < 0.05$ versus EMC of all the time points. (D) Representative immunohistochemical images of defect areas. IFN-γ positive cells were highly expressed in the EMC scaffolds while the IMC scaffolds showed a profoundly expression of IL-4.

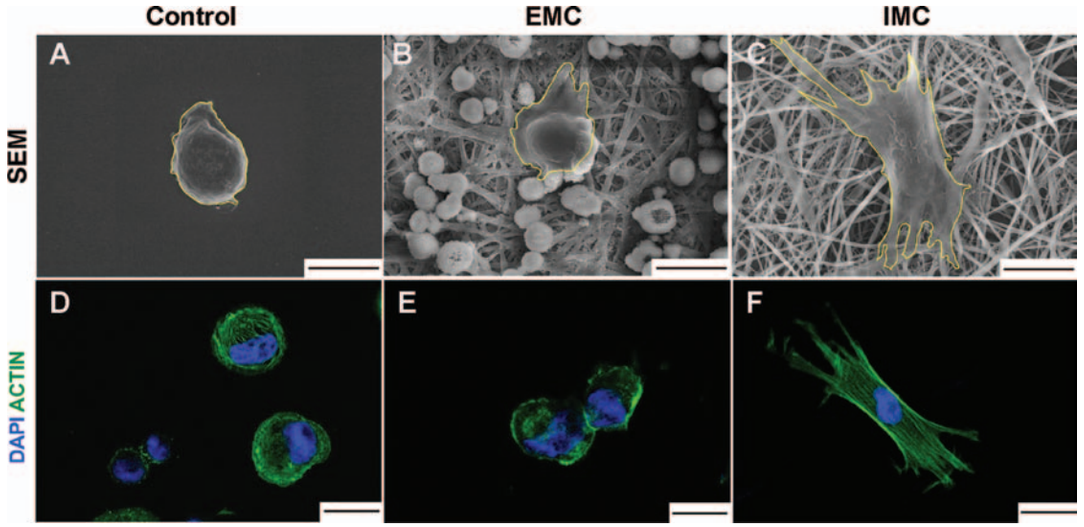

Figure 5. Macrophage morphology seeded on mineralized collagen scaffolds by SEM (A–C) and LSM (D–F). The macrophage seeded on the glass slide (A) showed a sphere-like appearance. The macrophages seeded on the EMC scaffold (B) and the IMC (C) scaffold adhered to the surface of the scaffolds well. However, the apatite clusters in the EMC scaffold seemed to impair the macrophage elongation and migration while in the IMC group macrophages extended more freely and tended to have a polarized morphology. The representative images of actin immunofluorescence staining, consistent with the SEM, showed that macrophages on the EMC scaffold (E) remained a round, oval shape whereas on the IMC scaffold (F) appeared a spindle-like polarized shape. Scale bar = 10 μm (A–C), 20 μm (D–E).

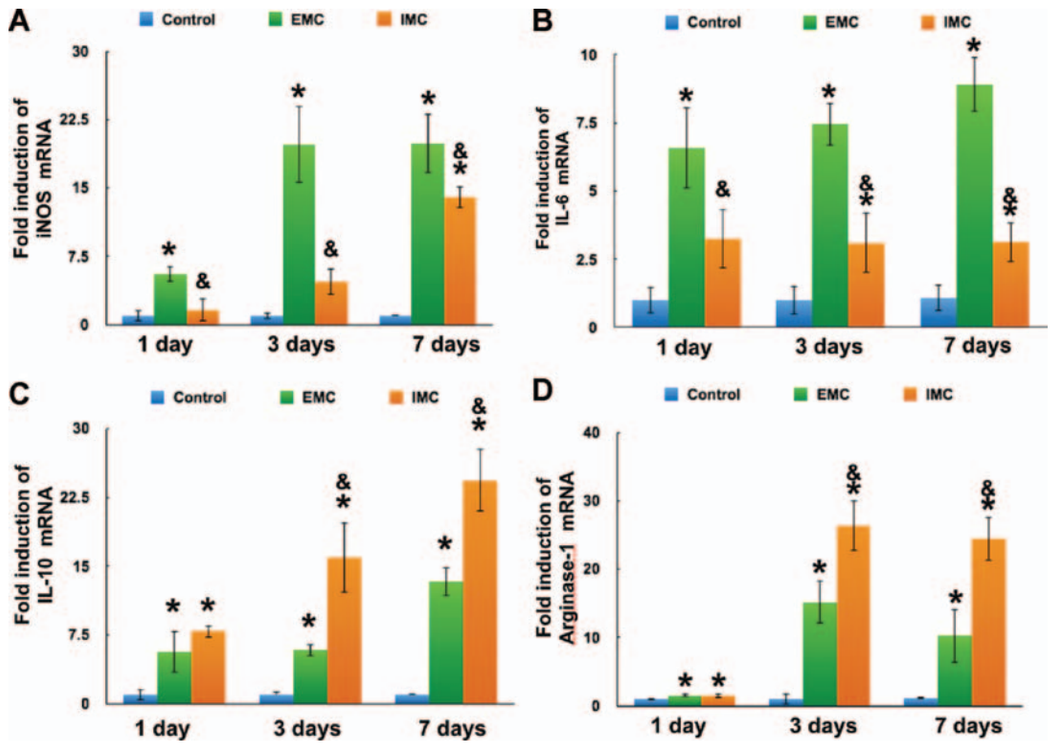

Figure 6. Relative mRNA expression levels of macrophage-polarization related genes at 1, 3, 7 days. (A) iNOS. (B) IL-6. (C) IL-10. (D) Arginase-1. The M1 macrophage related pro-inflammatory genes (A, B) were significantly upregulated in the EMC group. However, the M2 macrophage related anti-inflammatory genes (C, D) expression levels were much more upregulated in the IMC group. For each time point, $^{*}P < 0.05$ versus control; $^{\&}P < 0.05$ versus EMC group.

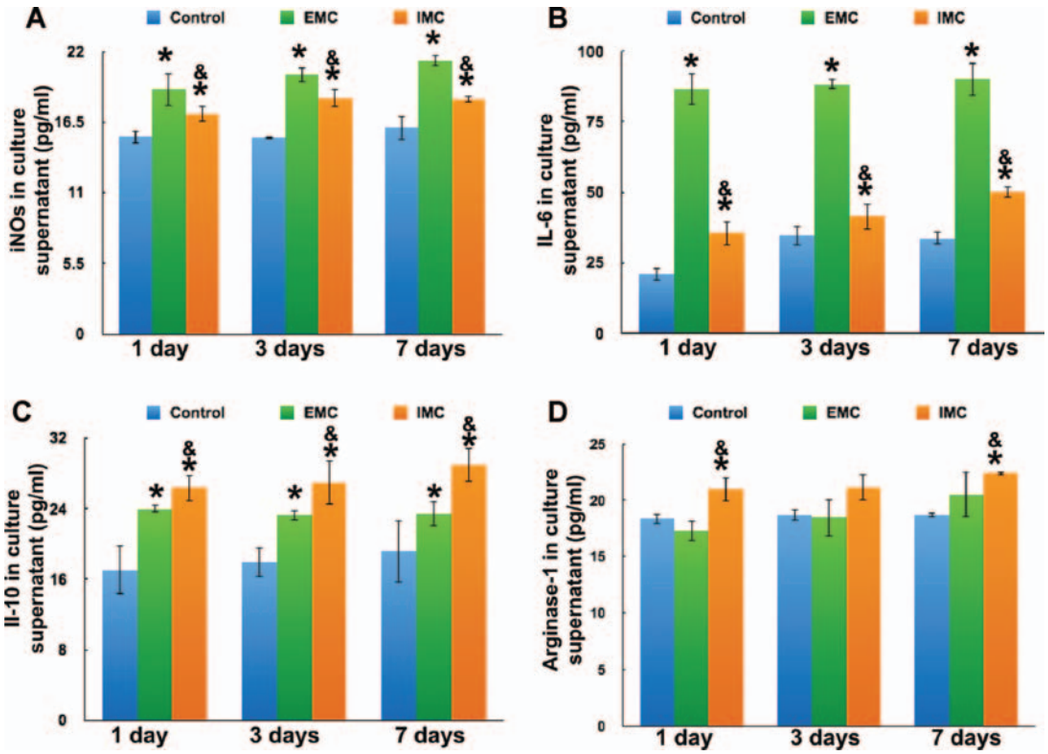

Figure 7. **Secretion of macrophage associated cytokines at 1, 3, 7 days. (A) iNOS. (B) IL-6. (C) IL-10. (D) Arginase-1. M1 marker (A, B), remained a significantly high level of secretion in the EMC group, while the concentrations of M2 marker (C, D) increased dramatically in the IMC group. $^{*}P < 0.05$ versus control; $^{\&}P < 0.05$ versus EMC group.**

has been established on which phenotype is more beneficial to osteogenesis. Some studies report that the pro-inflammatory M1, not the anti-inflammatory M2 macrophages induce osteogenesis of BMSCs.[57] However, other studies show that the M1 macrophages could induce osteoblasts to differentiate towards fibroblasts[58] and the M2 macrophages might contribute to enhance osteogenesis due to the secretion of osteoinductive and osteogenic cytokines such as transforming growth factor-β.[59] In our study, we found that the IMC-simulated macrophages showed an effective shift to the M2 polarization and enhanced the expression levels of osteogenic genes (ALP, OCN, RUNX2) of hBMSCs. This is consistent with previous studies[51, 52, 59, 60] in which macrophage-conditioned biomaterials extracts enhance the osteogenic differentiation of BMSCs. Taken together, the IMC scaffold could modulate the immune microenvironment by polarizing macrophages towards M2 phenotype and promote the hBMSCs to differentiate towards osteoblasts, which might finally lead to a better bone regeneration outcome.

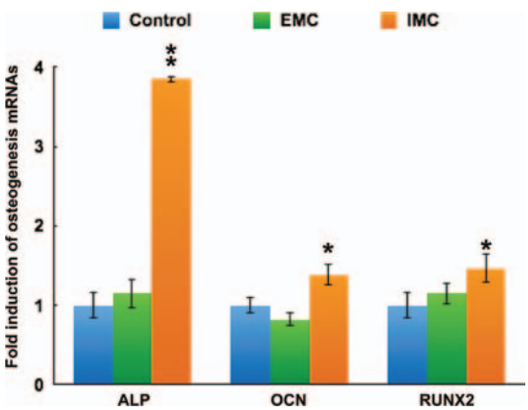

Figure 8. **Relative mRNA expression levels of osteogenic differentiation markers of hBMSCs. The IMC-stimulated macrophages significantly enhanced the mRNA expression levels of ALP, OCN, and RUNX2 of hBMSCs. $^{*}P < 0.05$ versus control; $^{**}P < 0.01$ versus control.**

CONCLUSIONS

In summary, the nanostructure of mineralized collagen scaffolds regulates macrophage polarization during bone regeneration. The IMC scaffold, mimicking the nanostructure of natural bone, could modulate host immune response by provoking a significantly effective and adequate M2 macrophage polarization, both *in vivo* and *in vitro*, and presented a better outcome of bone regeneration. This nanostructure-induced macrophage polarization provides an idea for predicting the performance of biomaterials after implantation, indicating that immunomodulatory properties should be taken in concern when evaluating bone substitute biomaterials. Further studies are needed

to illuminate the mechanism of macrophage polarization induced by surface nanotopography and also the crosstalks between the polarized macrophages and osteogenisis of BMSCs.

Acknowledgments: This work was supported by National Natural Science Foundations of China (81201198, 81400561) and Beijing Municipal Natural Science Foundation (7152156). The authors declare no potential conflicts of interest with respect to the authorship and/or publication of this article.

REFERENCES

1. R. R. Betz, Limitations of autograft and allograft: New synthetic solutions. *Orthopedics* 25, 561 **(2002)**.
2. W. L. Grayson, M. Frohlich, K. Yeager, S. Bhumiratana, M. E. Chan, C. Cannizzaro, L. Q. Wan, X. S. Liu, X. E. Guo, and G. Vunjak-Novakovic, Engineering anatomically shaped human bone grafts. *Proc. Natl. Acad. Sci. USA* 107, 3299 **(2010)**.
3. J. D. Conway, Autograft and nonunions: Morbidity with intramedullary bone graft versus iliac crest bone graft. *Orthop. Clin. North Am.* 41, 75 **(2010)**.
4. S. F. Badylak and T. W. Gilbert, Immune response to biologic scaffold materials. *Semin. Immunol.* 20, 109 **(2008)**.
5. B. N. Brown and S. F. Badylak, Expanded applications, shifting paradigms and an improved understanding of host-biomaterial interactions. *Acta Biomater.* 9, 4948 **(2013)**.
6. C. A. Janeway and R. Medzhitov, Innate immune recognition. *Annu. Rev. Immunol.* 20, 197 **(2002).**
7. N. Fujiwara and K. Kobayashi, Macrophages in inflammation. *Curr. Drug Targets Inflamm. Allergy* 4, 281 **(2005)**.
8. F. O. Martinez, L. Helming, and S. Gordon, Alternative activation of macrophages: An immunologic functional perspective. *Annu. Rev. Immunol.* 27, 451 **(2009)**.
9. F. O. Martinez, A. Sica, A. Mantovani, and M. Locati, Macrophage activation and polarization. *Front. Biosci.* 13, 453 **(2008)**.
10. D. M. Mosser and J. P. Edwards, Exploring the full spectrum of macrophage activation. *Nat. Rev. Immunol.* 8, 958 **(2008)**.
11. A. Mantovani, S. K. Biswas, M. R. Galdiero, A. Sica, and M. Locati, Macrophage plasticity and polarization in tissue repair and remodeling. *J. Pathol.* 229, 176 **(2013)**.
12. C. Sima and M. Glogauer, Macrophage subsets and osteoimmunology: Tuning of the immunological recognition and effector systems that maintain alveolar bone. *Periodontol 2000* 63, 80 **(2013).**
13. D. M. Mosser, The many faces of macrophage activation. *J. Leukoc. Biol.* 73, 209 **(2003)**.
14. S. Gordon, Alternative activation of macrophages. *Nat. Rev. Immunol.* 3, 23 **(2003)**.
15. M. M. Hunter, A. Wang, K. S. Parhar, M. J. Johnston, N. Van Rooijen, P. L. Beck, and D. M. McKay, *In vitro*-derived alternatively activated macrophages reduce colonic inflammation in mice. *Gastroenterology* 138, 1395 **(2010)**.
16. B. M. Sicari, J. L. Dziki, B. F. Siu, C. J. Medberry, C. L. Dearth, and S. F. Badylak, The promotion of a constructive macrophage phenotype by solubilized extracellular matrix. *Biomaterials* 35, 8605 **(2014)**.
17. B. N. Brown, B. D. Ratner, S. B. Goodman, S. Amar, and S. F. Badylak, Macrophage polarization: An opportunity for improved outcomes in biomaterials and regenerative medicine. *Biomaterials* 33, 3792 **(2012)**.
18. S. F. Badylak, J. E. Valentin, A. K. Ravindra, G. P. McCabe, and A. M. Stewart-Akers, Macrophage phenotype as a determinant of biologic scaffold remodeling. *Tissue Eng. Part A* 14, 1835 **(2008).**
19. B. N. Brown, R. Londono, S. Tottey, L. Zhang, K. A. Kukla, and M. T. Wolf, Macrophage phenotype as a predictor of constructive remodeling following the implantation of biologically derived surgical mesh materials. *Acta Biomater.* 8, 978 **(2012)**.
20. B. N. Brown, J. E. Valentin, A. M. Stewart-Akers, G. P. McCabe, and S. F. Badylak, Macrophage phenotype and remodeling outcomes in response to biologic scaffolds with and without a cellular component. *Biomaterials* 30, 1482 **(2009)**.
21. A. Mantovani, A. Sica, S. Sozzani, P. Allavena, A. Vecchi, and M. Locat, The chemokine system in diverse forms of macrophage activation and polarization. *Trends Immunol.* 25, 677 **(2004)**.
22. A. J. Rees, Monocyte and macrophage biology: An overview. *Semin. Nephrol.* 30, 216 **(2010)**.
23. J. M. Anderson, A. Rodriguez, and D. T. Chang, Foreign body reaction to biomaterials. *Semin. Immunol.* 20, 86 **(2008)**.
24. R. D. Stout, C. Jiang, B. Matta, I. Tietzel, S. K. Watkins, and J. Suttles, Macrophages sequentially change their functional phenotype in response to changes in microenvironmental influences. *J. Immunol.* 175, 342 **(2005)**.
25. R. D. Stout and J. Suttles, Functional plasticity of macrophages: Reversible adaptation to changing microenvironments. *J. Leukoc. Biol.* 76, 509 **(2004)**.
26. S. Franz, S. Rammelt, D. Scharnweber, and J. C. Simon, Immune responses to implants—A review of the implications for the design of immunomodulatory biomaterials. *Biomaterials* 32, 6692 **(2011)**.
27. J. A. Hubbell, S. N. Thomas, and M. A. Swartz, Materials engineering for immunomodulation. *Nature* 462, 449 **(2009)**.
28. P. D. Dwivedi, A. Tripathi, K. M. Ansari, R. Shanker, and M. Das, Impact of nanoparticles on the immune system. *J. Biomed. Nanotechnol.* 7, 193 **(2011)**.
29. S. Weiner and H. D. Wagner, The material bone: Structure mechanical function relations. *Annu. Rev. Mater. Sci.* 28, 271 **(1998)**.
30. K. L. Spiller, S. Nassiri, C. E. Witherel, R. R. Anfang, J. Ng, K. R. Nakazawa, T. Yu, and G. Vunjak-Novakovic, Sequential delivery of immunomodulatory cytokines to facilitate the M1-to-M2 transition of macrophages and enhance vascularization of bone scaffolds. *Biomaterials* 37, 194 **(2015)**.
31. R. Roy, A. Tripathi, M. Das, and P. D. Dwivedi, Cytotoxicity and uptake of zinc oxide nanoparticles leading to enhanced inflammatory cytokines levels in murine macrophages: Comparison with bulk zinc oxide. *J. Biomed. Nanotechnol.* 7, 110 **(2011)**.
32. B. V. Fearing and M. E. Van Dyke, *In vitro* response of macrophage polarization to a keratin biomaterial. *Acta Biomater.* 10, 3136 **(2014)**.
33. D. P. Vasconcelos, M. Costa, I. F. Amaral, M. A. Barbosa, A. P. Águas, and J. N. Barbosa, Modulation of the inflammatory response to chitosan through M2 macrophage polarization using pro-resolution mediators. *Biomaterials* 37, 116 **(2015)**.
34. A. M. Rajam, P. Jithendr, A. B. Mandal, and C. Rose, Evaluation of *in vitro* macrophage response and *in vivo* host response to growth factors incorporated chitosan nanoparticle impregnated collagen-chitosan scaffold. *J. Biomed. Nanotechnol.* 10, 508 **(2014)**.
35. M. I. Khan, A. A. Sahasrabuddhe, G. Patil, M. J. Akhtar, M. Ashquin, and I. Ahmad, Nano-talc stabilizes TNF-alpha m-RNA in human macrophages. *J. Biomed. Nanotechnol.* 7, 112 **(2011)**.
36. Y. Liu, N. Li, Y. P. Qi, L. Dai, T. E. Bryan, J. Mao, D. H. Pashley, and F. R. Tay, Intrafibrillar collagen mineralization produced by biomimetic hierarchical nanoapatite assembly. *Adv. Mater.* 23, 975 **(2011)**.
37. Y. Liu, Y. K. Kim, L. Dai, N. Li, S. O. Khan, D. H. Pashley, and F. R. Tay, Hierarchical and non-hierarchical mineralization of collagen. *Biomaterials* 32, 1291 **(2011)**.
38. Y. Liu, D. Luo, X. X. Kou, X. D. Wang, F. R. Tay, Y. L. Sha, Y. H. Gan, and Y. H. Zhou, Hierarchical intrafibrillar nano-carbonated apatite assembly improves nanomechanics and cytocompatibility of mineralized collagen. *Adv. Funct. Mater.* 23, 1404 **(2013)**.
39. Y. Liu, D. Luo, S. Liu, Y. Fu, Y. L. Sha, Y. H. Gan, and Y. H. Zhou, Effect of nanostructure of mineralized collagen scaffolds

on their physical properties and osteogenic potential. *J. Biomed. Nanotechnol.* 10, 1049 **(2014)**.
40. L. B. Kaban, J. Glowacki, and J. E. Murray, Repair of experimental mandibular bony defects in rats. *Surg. Forum* 30, 519 **(1979)**.
41. J. O. Hollinger and J. C. Kleinschmidt, The critical size defect as an experimental model to test bone repair materials. *J. Craniofacial Surg.* 1, 60 **(1990)**.
42. S. O. Akintoye, T. Lam, S. T. Shi, J. Brahim, M. T. Collins, and P. G. Robey, Skeletal site-specific characterization of orofacial and iliac crest human bone marrow stromal cells in same individuals. *Bone* 38, 758 **(2006)**.
43. S. Franz, S. Rammelt, D. Scharnweber, and J. C. Simon, Immune responses to implants: A review of the implications for the design of immunomodulatory biomaterials. *Biomaterials* 32, 6692 **(2011)**.
44. S. A. Eming, M. Hammerschmidt, T. Krieg, and A. Roers, Interrelation of immunity and tissue repair or regeneration. *Semin. Cell Dev. Biol.* 20, 517 **(2009)**.
45. S. Rukmani, R. C. Andrew, D. J. Kelly, C. J. Kearney, and F. J. O'Brien, Biomaterial based modulation of macrophage polarization: A review and suggested design principles. *Mater. Today* 18, 313 **(2015)**.
46. B. N. Brown and S. F. Badylak, Expanded applications, shifting paradigms and an improved understanding of host-biomaterial interactions. *Acta Biomater.* 9, 4948 **(2013)**.
47. K. Garg, N. A. Pullen, C. A. Oskeritzian, J. J. Ryan, and G. L. Bowlin, Macrophage functional polarization (M1/M2) in response to varying fiber and pore dimensions of electrospun scaffolds. *Biomaterials* 34, 4439 **(2013)**.
48. S. Chen, J. A. Jones, Y. Xu, H. Y. Low, J. M. Anderson, and K. W. Leong, Characterization of topographical effects on macrophage behavior in a foreign body response model. *Biomaterials* 31, 3479 **(2010)**.
49. Q. L. Ma, L. Z. Zhao, and R. R. Liu, Improved implant osseointegration of a nanostructured titanium surface via mediation of macrophage polarization. *Biomaterials* 35, 9853 **(2014)**.
50. Z. Chen, C. Wu, W. Gu, T. Klein, R. Crawford, and Y. Xiao, Osteogenic differentiation of bone marrow MSCs by β-tricalcium phosphate stimulating macrophages via BMP2 signalling pathway. *Biomaterials* 35, 1507 **(2014)**.
51. Z. Chen, X. Mao, L. Tan, T. Friis, C. Wu, R. Crawford, and Y. Xiao, Osteoimmunomodulatory properties of magnesium scaffolds coated with β-tricalcium phosphate. *Biomaterials* 35, 8553 **(2014)**.
52. K. L. Spiller, D. O. Freytes, and G. V. Novacovic, Macrophages modulate engineered human tissues for enhanced vascularization and healing. *Ann. Biomed. Eng.* 43, 616 **(2015)**.
53. K. A. Kigerl, J. C. Gensel, D. P. Ankeny, J. K. Alexander, D. J. Donnelly, and P. G. Popovich, Identification of two distinct macrophage subsets with divergent effects causing either neurotoxicity or regeneration in the injured mouse spinal cord. *J. Neurosci.* 29, 13435 **(2009)**.
54. J. E. Valentin, A. M. Stewart-Akers, T. W. Gilbert, and S. F. Badylak, Macrophage participation in the degradation and remodeling of extracellular matrix scaffolds. *Tissue Eng. Part A* 15, 1687 **(2009)**.
55. S. Lee, J. Choi, S. Shin, Y. M. Im, J. Song, and S. S. Kang, Analysis on migration and activation of live macrophages on transparent flat and nanostructured titanium. *Acta Biomater.* 7, 2337 **(2011)**.
56. F. Y. McWhorter, T. Wang, P. Nguyen, T. Chung, and W. F. Liu, Modulation of macrophage phenotype by cell shape. *Proc. Natl. Acad. Sci.* 110, 17253 **(2013)**.
57. P. Guihard, Y. Danger, B. Brounais, E. David, R. Brion, J. Delecrin, C. D. Richards, S. Chevalier, F. Rédini, D. Heymann, H. Gascan, and F. Blanchard, Induction of osteogenesis in mesenchymal stem cells by activated monocytes/macrophages depends on oncostatin M signaling. *Stem Cells* 30, 762 **(2012)**.
58. C. M. Champagne, J. Takebe, S. Offenbacher, and L. F. Cooper, Macrophage cell lines produce osteoinductive signals that include bone morphogenetic protein-2. *Bone* 30, 26 **(2002)**.
59. D. O. Freytes, J. W. Kang, I. Marcos-Campos, and G. Vunjak-Novakovic, Macrophages modulate the viability and growth of human mesenchymal stem cells. *J. Cell Biochem.* 114, 220 **(2013)**.